A Six-Body Potential Energy Surface for the S_N2 Reaction $Cl^-(g) + CH_3Cl(g)$ and a Variational Transition-State-Theory Calculation of the Rate Constant

Susan C. Tucker and Donald G. Truhlar*

Contribution from the Department of Chemistry and Supercomputer Institute, University of Minnesota, Minneapolis, Minnesota 55455-0431. *Received July 24, 1989*

Abstract: Correlated calculations (MP2/6-31G**) of the energies and frequencies at the saddle point, ion–dipole complex, and reactants plus additional energy calculations at selected geometries in the strong interaction region are used to parameterize a multidimensional potential energy function for the title reaction. Semiclassical variational transition-state theory is used to calculate the gas-phase rate coefficient and to determine a semiempirical value of the barrier height to reproduce the experimental value of this coefficient at 300 K. The semiempirical gas-phase barrier height is 3.1 kcal/mol. A new potential energy function with this barrier height is created and used to calculate the temperature-dependent rate coefficients and phenomenological activation energies for both CH_3Cl and CD_3Cl over the 200–1000 K temperature range. The activation energy is predicted to show a large temperature dependence. The kinetic isotope effect is predicted to be 1.04 at room temperature.

1. Introduction

The change in reaction rate upon solvation for halide plus methyl halide bimolecular nucleophilic substitution (S_N2) is dramatic—the aqueous-phase rate coefficients are many orders of magnitude slower than the corresponding gas-phase ones.[1-4] The halide–methyl halide reactions thus present a good test of our ability to model solvent effects on reactivity. We specifically consider the methyl exchange between chloride and methyl chloride[5-16]

$$Cl^- + CH_3Cl' \rightarrow ClCH_3 + Cl'^- \qquad (R1)$$

because its aqueous-phase solvation effects have been so widely studied in previous theoretical work, including Monte Carlo simulation techniques,[6,7] generalized Langevin theory and molecular dynamics,[8,12] the extended RISM integral equation method,[14] and continuum solvation models.[11,13,15] However, none of the studies mentioned above treats reaction R1 in its full dimensionality. The general procedure has been to treat the methyl group as a single body in the force field, although, for example, Chandrasekhar et al.[6] used four sites on a rigid methyl group to model the methyl–water interactions, Jorgensen and Buckner[7] considered all atoms explicitly in their ab initio study of the effect of hydration on the chloride–methyl chloride symmetric stretch, and Hwang et al.[10] included methyl halogens by molecular mechanics in their empirical valence bond model. Since the methyl group umbrella mode is strongly coupled to the reaction coordinate in Walden inversion reactions like R1, it may be a serious approximation to ignore these effects. Thus, in this paper we present a full multidimensional potential energy function for the gas-phase reaction R1. This surface should be of general usefulness for a variety of model studies. For example in the following paper,[17] we address the issue of adding water molecules to the system by using the present potential energy function plus solute–solvent and solvent–solvent interactions to study both the static and the dynamic solvation effects of microsolvation, and we discuss the resultant dynamics in relation to the concept of nonequilibrium solvation. In addition, Vande Linde and Hase[16] have recently made a preliminary communication of a gas-phase trajectory study of the effect of vibrational excitation of CH_3Cl on the cross section for reaction R1 based on an unpublished global potential energy surface, and the present potential energy surface can also be used to study vibrational enhancement of reactivity.

In section 2 we present a potential energy function for reaction R1. In section 3 we discuss the salient features of this function, which is called V_A to emphasize the largely ab initio character of its saddle point characteristics, and we also discuss the gas-phase kinetics in terms of this function. In section 4 we discuss another function, V_S, which is semiempirically adjusted to give a more accurate rate constant. Section 5 contains concluding remarks.

2. The Potential Energy Function

2.1. Overview. Our analytic potential energy function, V_A, for reaction R1 is based on partitioning the potential into separate, simpler interactions which are summed to give the total potential for a given geometric configuration. First we separate the potential into a three-body term, V^{3B}, which treats the methyl group as a single particle, and a vibrational term, V^{vib}, which adds the potential due to the hydrogen vibrations. Thus

$$V_A = V^{3B} + V^{vib} \qquad (1)$$

The three-body term represents the main part of the gas-phase potential for a particular configuration of the three-body system (r_{12}, r_{23}, r_{31}; See Figure 1) when the hydrogens are in or near their local equilibrium positions for the given geometry of the heavier atoms. The vibrational term V^{vib} accounts for the deviations of the hydrogens from their local equilibrium positions, and, in addition, we improve the representation of some of the vibrations included in V^{3B}, e.g., the Cl–C–Cl bends, in this term.

The three-body part, V^{3B}, includes the forces responsible for bond breaking and bond making and is anharmonic. The vibrational potential, V^{vib}, is a harmonic potential in Cartesian coordinates. It is based on ab initio calculations of the full $3N \times 3N$ matrix of Cartesian second derivatives of the potential, where

(1) Tanaka, K.; Mackay, G. I.; Payzant, J. D.; Bohme, D. K. *Can. J. Chem.* **1976**, *54*, 1643.
(2) Olmstead, W. N.; Brauman, J. I. *J. Am. Chem. Soc.* **1977**, *99*, 4219.
(3) McLennan, D. J. *Aust. J. Chem.* **1978**, *31*, 1897.
(4) Albery, W. J.; Kreevoy, M. M. *Adv. Phys. Org. Chem.* **1978**, *16*, 85.
(5) Morokuma, K. *J. Am. Chem. Soc.* **1982**, *104*, 3732.
(6) Chandrasekhar, J.; Smith, S. F.; Jorgensen, W. L. *J. Am. Chem. Soc.* **1985**, *107*, 154.
(7) Jorgensen, W. L.; Buckner, J. K. *J. Phys. Chem.* **1986**, *90*, 4651.
(8) Bergsma, J. P.; Gertner, B. J.; Wilson, K. R.; Hynes, J. T. *J. Chem. Phys.* **1987**, *86*, 1356.
(9) Bash, P. A.; Field, M. J.; Karplus, M. *J. Am. Chem. Soc.* **1987**, *109*, 8092.
(10) Hwang, J.-K.; King, G.; Creighton, S.; Warshel, A. *J. Am. Chem. Soc.* **1988**, *110*, 5297.
(11) Lee, S.; Hynes, J. T. *J. Chem. Phys.* **1988**, *88*, 6853.
(12) Gertner, B. J.; Wilson, K. R.; Hynes, J. T. *J. Chem. Phys.* **1989**, *90*, 3537.
(13) Kozaki, T.; Morihashi, K.; Kikuchi, O. *J. Am. Chem. Soc.* **1989**, *111*, 1547.
(14) Huston, S. E.; Rossky, P. J.; Zichi, D. A. *J. Am. Chem. Soc.* **1989**, *111*, 5680.
(15) Tucker, S. C.; Truhlar, D. G. *Chem. Phys. Lett.* **1989**, *157*, 164.
(16) Vande Linde, S. V.; Hase, W. L. *J. Am. Chem. Soc.* **1989**, *111*, 2349.
(17) Tucker, S. C.; Truhlar, D. G. Following paper in this issue.

0002-7863/90/1512-3338$02.50/0

N is the number of atoms (six); the resulting analytic potential function includes force constants for all cross-term interactions. Thus, by using this formalism, we make no assumptions about which mode–mode interactions are important and which can be neglected. They are all included, at least through quadratic terms.

Before describing the analytic fit in detail, we briefly review the relevant ab initio and experimental data that we require our analytic fit to emulate. Ab initio calculations for the stationary points, which were performed with the present fit in mind, and a more complete survey of the experimental results have been given in a previous paper.[18] Additional calculations at the MP2/6-31G** level (we use standard notation[19] for ab initio methods and basis sets) were performed at nonstationary points expressly for the present fit, and these are discussed in section 2.3 and 2.4 below.

The reaction path for R1 is a symmetric double well potential with five stationary points: reactants ($\mathcal{R}$); a charge–dipole complex ($\mathcal{C}$), which is lower in energy than $\mathcal{R}$, between $\mathcal{R}$ and the transition state; the transition state (‡) which is higher in energy than $\mathcal{R}$; a complex ($\mathcal{C}'$) between ‡ and products; and products, ($\mathcal{P}$). By symmetry, $\mathcal{R}$ and $\mathcal{P}$ are equivalent and $\mathcal{C}$ and $\mathcal{C}'$ are equivalent. Thus, we discuss only the three distinct stationary points $\mathcal{R}$, $\mathcal{C}$ and ‡.

Our best ab initio calculations[18] were performed at the MP2/6-31G** level. They yield a complexation energy of −10.8 kcal/mol, including a potential energy contribution of −11.0 kcal/mol and a zero point contribution of +0.2 kcal/mol estimated from scaled harmonic frequencies;[18] the theoretical complexation energy may be compared to the apparently best experimental value[20] of −12.2 ± 2 kcal/mol; it agrees within experimental error. Our best ab initio value for the energy, $\Delta E^{\ddagger}$, of ‡ with respect to $\mathcal{R}$, is 4.5 kcal/mol, which appears to be slightly high.[18] By using conventional transition-state theory, our best ab initio geometries, and our best scaled ab initio vibrational frequencies, we found[18] that a barrier of 3 kcal/mol reproduces the experimental[21] rate constant for this reaction. This indicates that the error in the ab initio energies is small. Thus, in the present article, we will present two analytic functions, the first of which, called V_A, is fit entirely to the MP2/6-31G** ab initio data and the second of which, called V_S, is similar but has a quantitatively small semiempirical modification such that generalized transition-state theory including semiclassical tunneling yields the experimental rate constant of 300 K. We note that V_A and V_S are related in an additive fashion, i.e.,

$$V_S = V_A + V_\delta \tag{2}$$

where V_δ will be defined later, and that the main difference between the surfaces is in their saddle point heights, 4.5 kcal/mol for surface A and 3.1 kcal/mol for surface B.

In addition to the energy levels at the three stationary points, surface A is required to reproduce, to reasonable accuracy, the scaled ab initio frequencies from our best ab initio calculations[18] at these points plus one other point. For potential function V_S, the frequencies at ‡ (especially the asymmetric stretch) are varied from the scaled ab initio values in a way that may correct for the same systematic error as presumably effects the ab initio barrier height.

In section 2.2 we describe the form of the three-body potential, V^{3B}, and in section 2.3 we give the parameters and briefly describe the fitting procedure. In section 2.4 we describe the form of V^{vib} and how it is interfaced with V^{3B} to ensure that the sum, V_A, satisfies the fit requirements. For V^{vib}, details regarding the parameter values and how they were chosen are relegated to appendices which are submitted as Supplementary Material.

2.2. The Three-Body Potential V^{3B}. We use the convention that Me denotes the CH_3 fragment; thus we write $[Cl\cdots Me\cdots Cl]^-$ for the three-body model of the charged six-body system. In order to develop the potential surface for this system, we first consider the neutral analog, $[Cl\cdots Me\cdots Cl]^-$, which is described by a generalized,[22-24] extended[25] LEPS[26] (London–Eyring–Polanyi–Sato) function, V^{LEPS}. (The LEPS method is a form of semiempirical valence bond theory. The extended LEPS formulation[25] differs from the original[26] LEPS method in that the Sato parameters are not required to be the same for all diatomic pairs; the further generalization[22-24] consists in making the Sato parameters functions of geometry rather than constants.) To describe the difference between the charged and neutral system, we use a sum, called V^{LR}, of pairwise charge–charge and charge–polarizability terms which are cut off at short distances.[27] Thus, V^{3B} is given by

$$V^{3B} = V^{LEPS} + V^{LR} + V^0 \tag{3}$$

where V^0 is a constant which is added such that $V^{3B} = 0$ at the classical equilibrium geometry in both the asymptotic reactants and products regions. Our fit contains a total of eight semiempirically adjusted parameters (see below), four in V^{LEPS} and four in V^{LR}. All eight parameters were adjusted simultaneously, as discussed in section 2.3.

2.2.1. LEPS Potential. The three-body extended LEPS potential V^{LEPS} is comprised, in the standard manner, of approximations Q_{ij} and J_{ij} to the Coulomb and exchange integrals, respectively, for the three "diatomic" pairs, ClMe, MeCl′, and ClCl′. In particular[25,28]

$$V^{LEPS} = Q_{12}(r_{12}) + Q_{23}(r_{23}) + Q_{13}(r_{13}) - \left\{\frac{1}{2}[(J_{12}(r_{12}) - J_{23}(r_{23}))^2 + (J_{23}(r_{23}) - J_{13}(r_{13}))^2 + (J_{13}(r_{13}) - J_{12}(r_{12}))^2]\right\}^{1/2} \tag{4}$$

where 1 ≡ Cl, 2 ≡ Me, 3 ≡ Cl′, and Q_{ij} and J_{ij} are given by

$$Q_{ij} = \frac{1}{2}\left[{}^1V_{ij}(r_{ij}) + \frac{(1 - \Delta_{ij})}{(1 + \Delta_{ij})}{}^3V_{ij}(r_{ij})\right] \tag{5}$$

and

$$J_{ij} = \frac{1}{2}\left[{}^1V_{ij}(r_{ij}) - \frac{(1 - \Delta_{ij})}{(1 + \Delta_{ij})}{}^3V_{ij}(r_{ij})\right] \tag{6}$$

where Δ_{ij} are the Sato parameters (see below), and ${}^1V_{ij}$ and ${}^3V_{ij}$ are approximate singlet and triplet energy functions for the diatomic pairs given by

Table I. Morse Parameters for the Neutral "Diatomics" MeCl and Cl_2

	MeCl	Cl_2
D_{ij} (kcal/mol)	86.5[a]	58.0[b]
β_{ij} (Å^{-1})	1.66[c]	2.00[d]
r^0_{ij} (Å)	1.78[e]	1.988[b]

[a] D_0 evaluated from ref 29 by a thermodynamic cycle. D_e, which is the appropriate dissociation energy for eqs 7 and 8, is evaluated by $D_e = D_0 + {}^1/_2hc\{\sum_i \nu_i^{CH_3Cl} - \sum_i \nu_i^{CH_3}\}$ where $\nu_i^{CH_3Cl}$ are from ref 30 and $\nu_i^{CH_3}$ are from refs 31 and 32. [b] D_e and r^0 from ref 34. [c] β is calculated from ν_3 by assuming the Me–Cl motion and the hydrogen motions ar separable. We write the reduced mass as $\mu = m_{Me}m_{Cl}/(m_{Me} + m_{Cl})$ allowing the calculation of the harmonic force constant. The second derivative of the Morse curve, $2D_e\beta^2$, is equated with the harmonic force constant to yield β. [d] β is evaluated by equating the harmonic force constant—evaluated from the harmonic frequency in ref 34—with the second derivative of the Morse curve, $2D_e\beta^2$. [e] r^0 from ref 33.

(18) Tucker, S. C.; Truhlar, D. G. *J. Phys. Chem.* **1989**, *93*, 8138.
(19) Hehre, W. J.; Radom, L.; Schleyer, P. v. R.; Pople, J. A. *Ab Initio Molecular Orbital Theory*; John Wiley and Sons: New York, 1986.
(20) Larson, J. W.; McMahon, T. B. *J. Am. Chem. Soc.* **1984**, *106*, 517.
(21) Barlow, S. E.; VanDoren, J. M.; Bierbaum, V. M. *J. Am. Chem. Soc.* **1988**, *106*, 7240.
(22) Blais, N. C.; Truhlar, D. G. *J. Chem. Phys.* **1974**, *61*, 4186.
(23) Truhlar, D. G.; Garrett, B. C.; Blais, N. C. *J. Chem. Phys.* **1984**, *80*, 232.
(24) Brown, F. B.; Steckler, R.; Schwenke, D. W.; Truhlar, D. G.; Garrett, B. C. *J. Chem. Phys.* **1985**, *82*, 188.
(25) Kuntz, P. J.; Nemeth, E. M.; Polanyi, J. C.; Rosner, S. D.; Young, C. E. *J. Chem. Phys.* **1966**, *44*, 1168.
(26) Sato, S. *J. Chem. Phys.* **1955**, *23*, 592.
(27) Moran, T. F.; Hamill, W. H. *J. Chem. Phys.* **1963**, *39*, 1413.
(28) Blais, N. C. Technical report no. LA-4603, Los Alamos Scientific Laboratory, Los Alamos, NM, April 1971.

$$^1V_{ij} = D_{ij}[e^{-2\beta_{ij}(r_{ij}-r^0_{ij})} - 2e^{-\beta_{ij}(r_{ij}-r^0_{ij})}] \quad (7)$$

and

$$^3V_{ij} = \frac{1}{2}D_{ij}[e^{-2\beta_{ij}(r_{ij}-r^0_{ij})} + 2e^{-\beta_{ij}(r_{ij}-r^0_{ij})}] \quad (8)$$

where r_{ij} is the distance between fragments i and j, with distances to the methyl group measured from the C atom. The parameters D_{ij}, β_{ij}, and r^0_{ij} were derived from experimental[29-34] values for the neutral "diatomic" pairs; these values are given in Table I.

The Sato parameters Δ_{ij} in eqs 5 and 6 are adjusted semiempirically. Because variation of Δ_{13} causes only small changes in the potential in the vicinity of the reaction path, it does not provide a useful fitting parameter, and we set it to zero in our fit. Notice that, due to symmetry, the ij = 12 and 23 "diatomic" pairs both correspond to neutral Me–Cl, and thus they have the same parameters. Consequently, $\Delta_{12} = \Delta_{23}$, and we call this Δ_{MeCl}. We write Δ_{MeCl} as a function of r_{MeCl} for additional flexibility:

$$\Delta_{MeCl} = Z_{MeCl} + \frac{1}{2}\gamma_\Delta[1 + \tanh(a_\Delta(r_{MeCl} - \delta_\Delta))] \quad (9)$$

where Z_{MeCl}, γ_Δ, a_Δ, and δ_Δ are the four semiempirically adjustable parameters in V^{LEPS}. For the final values of a_Δ and δ_Δ, Δ_{MeCl} ranges from $\sim Z_{MeCl}$ to $(Z_{MeCl} + \gamma_\Delta)$ as r_{MeCl} goes from $r_{MeCl} \ll \delta_\Delta$ to ∞. The final values of these parameters are discussed in section 2.3. The motivation for making the Sato parameter Δ_{MeCl} be a function of r_{MeCl} is to make the long-range term attractive enough to give a well depth of −11 kcal/mol; without this feature attempts to increase the attraction by adjusting the parameters in the cutoff function led to values of r_{12} less than 3.1 Å. Simply making the Sato parameter Δ_{MeCl} larger (but still not a function of r_{MeCl}) lowers the van der Waals well, but it also leads to a spurious well along the symmetric stretch line through the saddle point. Making Δ_{MeCl} a function of r_{MeCl} according to eq 9 allows a fit having an appropriate value of Δ_{MeCl} in the saddle point region and a larger value of Δ_{MeCl} in the well region.

2.2.2. Long-Range Potential. The multipole-interaction contribution to the three-body potential is written as a function of the three internuclear distances (see Figure 1) and r_c, where r_c is a measure of reaction progress and is defined as[6]

$$r_c \equiv r_{23} - r_{12} \quad (10)$$

We write V^{LR} as a sum of pairwise interactions as follows:

$$V^{LR} = \sum_{i=1}^{2}\sum_{j=i+1}^{3} V^{LR}_{ij}[r_{ij},\{q_i(r_c,r_{13})\}]c(r_{ij}) \quad (11)$$

where c is a cutoff function included so that the long-range pairwise interactions go to zero at small distances. Although we require V^{LR} to be small (<0.6 kcal/mol) in the reactants region, we do not require it to be zero. The set "q_i" appearing in eq 11 denotes the values (q_1, q_2, q_3) of nominal charge parameters for Cl, Me, and Cl′, respectively. These charge parameters are called nominal because they are not necessarily claimed to represent physical charges; they are merely parameters of the potential energy function and do not have to be interpreted as charges except to motivate the functional form of the potential.

The cutoff function c is given by

$$c = \left\{\frac{1}{2} + \frac{1}{2}\tanh[a_c(r_{ij} - \delta_c)]\right\}^2 \quad (12)$$

where a_c and δ_c, which govern its range and origin, respectively, are semiempirically adjustable parameters; their final values are discussed in section 2.3.

The interaction terms are given as

$$V^{LR}_{ij} = \frac{q_i(r_c,r_{13})q_j(r_c,r_{13})}{r_{ij}} - \frac{\alpha_i(q_i(r_c,r_{13}))q_j(r_c,r_{13})^2}{2r_{ij}^4} - \frac{\alpha_j(q_j(r_c,r_{13}))q_i(r_c,r_{13})^2}{2r_{ij}^4} \quad (13)$$

Table II. Fixed Charged Switching Parameters

γ_1	−1.0 e
γ_2	0.78 e
a_q	1.8 Å^{-1}

where α_i is the polarizability of group i (i = 1 for Cl, 2 for Me, and 3 for Cl′), and where the charge parameters are given by

$$q_1 = q_{Cl} = \gamma_1 + \frac{1}{2}\gamma_2\{1 + \tanh[f(r_{13})(r_c - \delta_q)]\} \quad (14)$$

with

$$f = a_q[1 - e^{-\beta_q r_{13}^2}] \quad (15)$$

$$q_2 = q_{Me} = -1 - q_1(r_c,r_{13}) - q_3(r_c,r_{13}) \quad (16)$$

and

$$q_3 = q_{Cl'} = q_1(-r_c,r_{13}) \quad (17)$$

where γ_1, γ_2, a_q, β_q are parameters described below. As pointed out in ref 8, the charges should be differentiable functions of geometry, and eqs 14 and 16 satisfy this criterion.

Notice that the width of the charge switching function, eq 14, depends on r_{13}, as shown in eq 15. Before making this modification, we had little separate control over the saddle point position and the well position. Our best fit with f equal to a constant a_q had a saddle point with $r_{12} = r_{23} = 2.3$ Å and a well with $r_{12} \cong 2.5$ Å instead of the desired 3.1 Å. The final functional form, eqs 14 and 15, contains the adjustable parameter β_q, which governs the change of the $\{q_i\}$ with r_{13}, and which has a large effect on the position of the van der Waals well.

The dependence, $f(r_{13})$, of the width of the charge switching functions on r_{13} was added to compensate for the inappropriateness of a point charge picture for tight configurations. We are at liberty to use this type of functional form since we are not interested in the value of the potential for the Cl–Cl–Me arrangement. The parameter β_q determines the degree to which q varies with r_{13}, and δ_q determines the value of the charge separation at $r_c = 0$. We allow δ_q to be an adjustable parameter because the surface is very sensitive to small changes in δ_q and because ab initio calculations do not define atomic charges uniquely. The final values of β_q and δ_q are discussed in section 2.3.

The values of γ_1, γ_2, and a_q are given in Table II. The parameters γ_1 and γ_2 were fixed such that the charges on the chlorines have the correct values in the asymptotic regions. For an isolated chlorine (e.g., Cl in the reactant region, Cl′ in the product region), the charge is −1.0 e. For the chlorine in isolated MeCl, we use the value −0.22 e, which was determined such that, for a two-body model of MeCl having a bond length of 1.79 Å, the calculated dipole moment matches the experimental value for MeCl, 0.39 eÅ.[35]

The value of a_q, which governs the rate of charge switching as a function of r_c, is determined from ab initio calculations. Chandrasekhar et al.[6] have performed geometry optimized HF/6-31G* calculations for this system at various fixed values of r_c. A least-squares fit of a hyperbolic tangent function to the charge on chlorine—from the Mulliken population analysis of the calculations of Chandrasekhar et al.[6]—as a function of r_c yields a width parameter of 1.8 Å^{-1}. Charge values from geometry optimized MP2/6-31G** ab initio calculations[18] at the saddle point and at the complex indicate that the slope of the charge

(29) Wagman, D. D.; Evans, W. H.; Parker, V. B.; Schumm, R. H.; Halow, I.; Bailey, S. M.; Churney, K. L.; Nuttall, R. L. *J. Phys. Chem. Ref. Dat.* **1982**, *11*, 1188.
(30) Shimanouchi, T. In *National Standard Reference Data Series, No. 39*; United States National Bureau of Standards: Washington, D.C., 1972; p 51.
(31) Jacox, M. E. *J. Phys. Chem. Ref. Data* **1984**, *13*, 945.
(32) Holt, P. L.; McCurdy, K. E.; Weisman, R. B.; Adams, J. S.; Engel, P. S. *J. Chem. Phys.* **1984**, *81*, 3349.
(33) Shull, D. R.; Prophet, H. *J.A.N.A.F. Tables*; 2nd ed.; 1971 and Suppl. 1977; NBS Nos. 37 and 48.
(34) Douglas, A. E.; Møler, Chr. Kn.; Stoicheff, B. P. *Can. J. Phys.* **1963**, *41*, 1174.
(35) *Handbook of Chemistry and Physics*, 63rd ed.; Weast, R. C., Ed.; The Chemical Rubber Company: Cleveland, OH, 1982; p E-60.

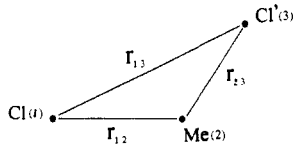

Figure 1. Coordinates used in the three-body potential, V^{3B}. The coordinates are internuclear distances with r_{12} and r_{23} being the distance from a Cl nucleus to the C nucleus.

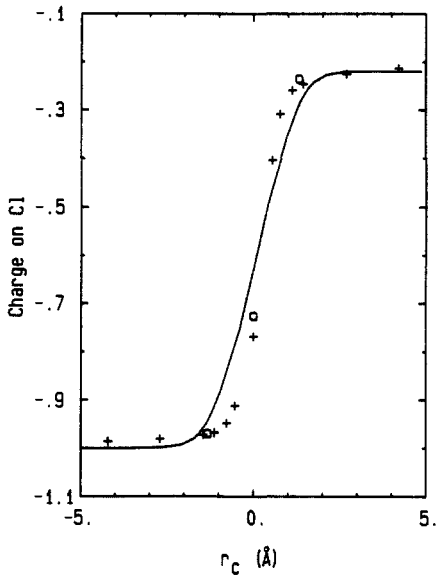

Figure 2. The charge, eq 14, in units of e on the incoming chlorine along the minimum energy path of the analytic fit V^{3B} plotted against r_c (solid line). Shown for comparison are the HF/6-31G* Mulliken population analysis charges of ref 6 (+) and the MP2/6-31G** Mulliken population analysis charges (□).

switching is nearly the same for the two methods. Also, the charge switching function for chlorine for this reaction reported by Kozaki et al.,[13] which was evaluated by the semiempirical MNDO method, appears to be very similar to the ab initio charge switching functions. Finally, during the fitting procedure, we checked to make sure that our surface is not very sensitive to the value of this parameter. Since it is not we used $a_q = 1.8$ Å^{-1} without further optimization. Figure 2 is a plot of the charge value of the incoming chlorine along the minimum energy path for the three-body potential V^{3B} as a function of r_c (solid line). Also shown are the HF/6-31G* charge values from Chandrasekhar et al.[6] (+ symbols) and the MP2/6-31G** values (□ symbols). Although we adjust a_q to the calculations of ref 6, the rate of charge switching of our fit, eq 14, differs slightly from those calculations because our fitted charge value depends on r_{13} as well as on r_c, eq 15, and r_{13} varies along the three-body minimum energy path.

The last function needed for eq 13 is the polarizability α_i. Because the polarizability of an ion can vary significantly from that of the corresponding atom or radical, we let the polarizability of each group be a function of the charge on that group, which itself is a function of r_c and r_{13}, eqs 14–17. Thus, by linear interpolation, we find

$$\alpha_1(q_1) = \alpha_{Cl} = \alpha^0_{Cl} - (\alpha^{ion}_{Cl} - \alpha^0_{Cl})q_1 \quad (18)$$

$$\alpha_{Cl'} = \alpha_3 = \alpha_1(q_3) \quad (19)$$

and

$$\alpha_2(q_2) = \alpha^0_{Me} - (\alpha^0_{Me} - \alpha^{ion}_{Me})q_2 \quad (20)$$

where α^0_{Cl}, α^{ion}_{Cl}, α^0_{Me}, and α^{ion}_{Me} are the polarizabilities of a neutral chlorine atom, a chloride ion, a methyl radical, and a methyl cation, respectively. The values[36-38] used for these parameters are given in Table III.

2.3. Fitting the Three-Body Potential, V^{3B}. The functional form proposed in the previous section has great flexibility by virtue of the eight adjustable parameters it contains, and these are adjusted to make our three-body surface realistic by fitting it to ab initio results. The eight parameters must be adjusted simultaneously because their values are coupled. Thus the fit parameters are adjusted in an iterative fashion. We list in Table IV the major effects of each of the eight parameters. In Table V we present

Table III. Polarizabilities

α^0_{Cl}	2.18 (Å^3)[a]
α^{ion}_{Cl}	4.68 (Å^3)[b]
$\alpha^0_{CH_3}$	2.28 (Å^3)[c]
$\alpha^{ion}_{CH_3}$	1.95 (Å^3)[c]

[a] From ref 36. [b] Calculated in ref 37 by the coupled Hartree–Fock method. [c] Calculated from the experimental value of α_{CH_4} (ref 38) by scaling for the total number of valence electrons, i.e., $\alpha^0_{CH_3} = (7/8)\alpha_{CH_4}$ and $\alpha^{ion}_{CH_3} = (6/8)\alpha_{CH_4}$.

Table IV. Major Effects of the Adjustable Parameters in V^{3B}

eq	parameter	properties affected[a]	eq	parameter	properties affected[a]
14	δ_q	V_{sp}, r_{sp}	9	γ_Δ	V_{vdw}, r_{vdw}
15	β_q	V_{sp}, r_{vdw}	9	a_Δ	V_{sp}, ν_{sym}
12	a_c	ν_{sym}, V^0	9	δ_Δ	V_{sp}, r_{vdw}, ν_i
12	δ_c	V_{sp}, r_{sp}, V^0	9	Z_{MeCl}	V_{sp}, r_{sp}

[a] V_{sp}, saddle point height; r_{sp}, saddle point position; ν_{sym}, saddle point symmetric stretch frequency; V^0, the value of V^{LR} ($r_{12} = 1.79$ Å, $r_{23} = r_{13} = \infty$); ν_i, imaginary frequency at the saddle point; V_{vdw}, the van der Waals well depth; r_{vdw}, max(r_{12},r_{23}) for the van der Waals well position.

Table V. Final Parameters and Properties for V^{3B}

eq	parameter	value	eq	parameter	value
14	δ_q	0.05 Å	9	γ_Δ	0.60
15	β_q	0.03 Å^{-2}	9	a_Δ	2.08 Å^{-1}
12	a_c	3.60 Å^{-1}	9	δ_Δ	2.73 Å
12	δ_c	1.973 Å	9	Z_{MeCl}	−0.155
			3	V^0	0.55149589 kcal/mol

property[a]	MP2/6-31G** results[b]	fit	% error
V_{sp}	4.5 kcal/mol	4.5 kcal/mol	0.0
r_{sp}	2.302 Å	2.302 Å	0.0
ν_{sym}	220 cm^{-1}	274 cm^{-1}	24.0
ν_i	485i cm^{-1}	452i cm^{-1}	6.8
V_{vdw}	−11.0 kcal/mol	−10.9 kcal/mol	0.9
$r_{vdw}(r_>)^c$	3.14 Å	3.14 Å	0.0
$r_{vdw}(r_<)^c$	1.81 Å	1.80 Å	0.6

[a] Quantities are as defined in Table IV. [b] From ref 18. [c] $r_> \equiv$ max(r_{12},r_{23}), $r_< \equiv$ min(r_{12},r_{23}).

Table VI. Reactant Properties for V^{3B}

quantity	V^{3B}	experiment	% error
r^0_{MeCl}	1.793 Å	1.781 Å[a]	0.7
ν_{MeCl}	665 cm^{-1}	732 cm^{-1} [b]	9.1

[a] Reference 34. [b] Reference 31.

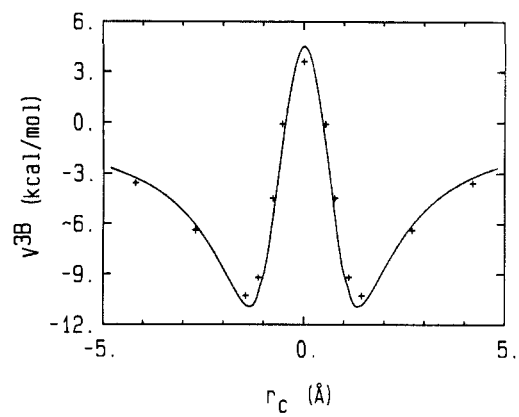

Figure 3. The potential energy along the minimum energy path of the analytic fit V^{3B} plotted against r_c (solid line). The HF/6-31G* values of ref 6 are shown for comparison (+).

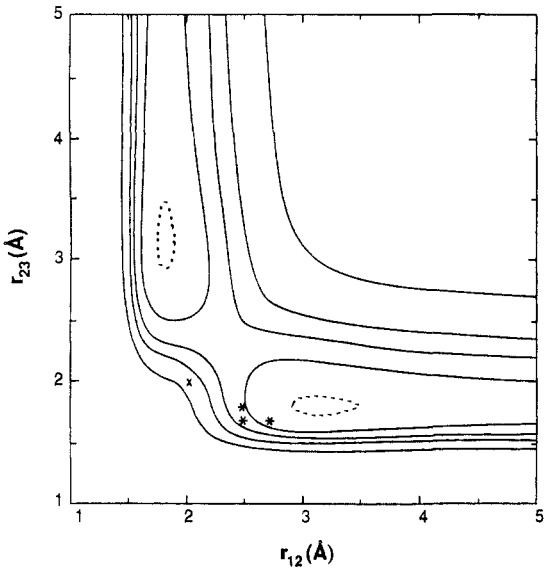

Figure 4. A contour plot of V^{3B} for collinear geometries, i.e., $r_{13} \equiv r_{12} + r_{23}$. Energy contours are at −10, 0, 10, 20, and 40 kcal/mol. Coordinate values and energies for the geometries denoted by × or * are given in Table VII.

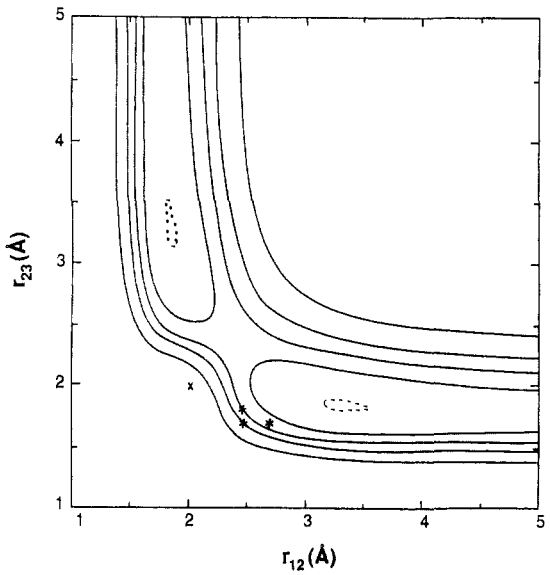

Figure 5. The same as Figure 4, except the potential of Bergsma et al. (ref 8).

the final values of these parameters. We also list the properties to which we fit, their desired values, and the values of these properties given by the analytic surface. In Table VI we compare properties of our surface in the reactants region with experimental values for MeCl. Figure 3 gives the potential along the minimum energy path (MEP) of the analytic surface V^{3B} as a function of r_c (each point on the MEP can be correlated with a unique value of r_c). For comparison we also show the HF/6-31G* values of Chandrasekhar et al.,[6] to which the model potential of Bergsma et al.[8] was fit.

In Figures 4 and 5 we compare the present three-body potential to the three-body potential of Bergsma et al.[8] at collinear geometries. The potential of Bergsma et al. has a much steeper symmetric stretch potential along the cut ($r_{12} = r_{23}$) which passes through the saddle point, a steeper ascent to the dissociation plateau, and a much higher value for the dissociation plateau (234.5 kcal/mol, as compared to our value, derived from experimental values, of 86.5 kcal/mol). In addition, the curvature of the MEP (and the shape of the surrounding valley) as it proceeds from the saddle point to the complex is quite different for the two potential functions. In order to ascertain which surface has the qualitatively correct behavior, we performed MP2/6-31G** calculations, for fixed r_{12}, r_{23}, and r_{13} and optimized hydrogen atom positions, at four points specially chosen in regions where the two surfaces differ significantly.

Table VII. Potential Fits and ab Initio Energies Evaluated at Four Nonstationary Points

		V^a (kcal/mol)				
r_{12} (Å)	r_{23} (Å)	Bergsma et al.[b]	V^{3B}	V_A[c]	V_S[d]	MP2/6-31G**
2.0	2.0[e]	84.3	31.0	26.3	24.9	26.4
2.45	1.8[e]	11.1	1.8	2.0	1.4	2.7
2.45	1.694[e]	20.1	5.2	6.2	5.7	9.7
2.678	1.694[e]	4.7	−3.7	−2.9	−3.1	−1.3

[a] Energies are given relative to reactants as the zero of energy. [b] Calculated from the gas-phase potential of ref 8. [c] Values for the multidimensional surface A, with r_{12} and r_{23} as given in the table and the hydrogens at their "equilibrium" positions, as determined by the set $\{x_i^0\}$. See section 3. [d] Same as previous column but for function V_S. [e] Note: $r_{13} = r_{12} + r_{23}$ for all points listed.

First, to determine which surface more accurately represents the symmetric stretch potential along the cut $r_{12} = r_{23}$, we evaluated the MP2/6-31G** energy at the point $r_{12} = r_{23} = 2.0$ Å, which is marked by an × in Figures 4 and 5; the result is reported, along with the values of the two fits at this point and the values of our two six-body functions V_A and V_S, defined in eqs 1 and 2 and discussed below, in Table VII. Then, to ascertain which surface best represents the shape of the MEP and the surrounding valley, we evaluated the MP2/6-31G** energy at the three points marked by asterisks in Figures 4 and 5 (r_{12} = 2.45 Å, r_{23} = 1.8 Å), (r_{12} = 2.45 Å, r_{23} = 1.694 Å), and (r_{12} = 2.678 Å, r_{23} = 1.694 Å). These energies as well as the fit and six-body values at these points are also given in Table VII.

At each of the four points in Table VII, the V^{3B} potential value is closer to the MP2/6-31G** value than is the value from the potential of Bergsma et al., indicating that the V^{3B} potential provides a better qualitative representation of the surface topology (at least in the regions considered important for the S_N2 reaction) than does the potential of Bergsma et al. In addition the final surface values are also reasonably close to the ab initio values, indicating that the additional terms in the full surfaces do not change the conclusion.

2.4. The Vibrational Potential V^{vib}. We write the vibrational potential, V^{vib}, as a harmonic potential in body-fixed Cartesian coordinates, $\{x_i\}_{i=1}^{18}$, i.e.,

$$V^{vib} = \frac{1}{2}\sum_{i=1}^{18}\sum_{j=1}^{18} k_{ij}(r_c)[x_i - x_i^0(r_c)][x_j - x_j^0(r_c)] \qquad (21)$$

where k_{ij} are the Cartesian harmonic force constants, and x_i^0 is the equilibrium value of Cartesian coordinate i. Because we are interested in evaluating V^{vib} for the case of a reacting system where bonds are being formed and broken, we account for the variation of the force constants, k_{ij}, and the equilibrium coordinate values, x_i^0, as the reaction proceeds by making them functions of r_c as defined by eq 10.

When fitting the set of equilibrium coordinate values, $\{x_i^0(r_c)\}$, we choose the origin of the body-fixed coordinate system to be at the carbon atom. Because we enforce C_{3v} symmetry along the reaction coordinate, the carbon and both chlorines lie along an axis, which we choose to be the z axis of the body-fixed coordinate system, and we choose the plane of this axis and one of the hydrogens to be the xz plane. To enforce C_{3v} symmetry, the equilibrium values of the remaining body-fixed coordinates are expressed in terms of the equilibrium values r_{12}^0, r_{23}^0, r_H^0, and θ^0, of four internal coordinates defined in Figure 6. The equilibrium values for these internal coordinates, which are functions of r_c, are required to yield values for the Cartesian equilibrium values $\{x_i^0(r_c)\}$ which match (to within 0.01 Å) the optimized ab initio geometries at the stationary points, and the values of r_{12}^0 and r_{23}^0 are required to closely approximate the minimum energy path (MEP) of the three-body potential, V^{3B}.

Since the ab initio carbon–hydrogen bond length varies by less than 0.02 Å from $\mathcal{R}$ to ‡, we let r_H^0 be a constant, equal to the

Table VIII. Parameters for the Set $\{x_i^0\}$

$\gamma_\theta = 18.5°$	$\gamma_r = 0.500\,801\,63$ Å
$a_\theta = 1.36$ Å^{-1}	$\beta_r = 2.444\,862\,73$ Å^{-2}
$A = 0.008\,044\,69$ Å	$r^0_{MeCl} = 1.793\,139\,54$ Å

average of the ab initio values, 1.07 Å. The MP2/6-31G** optimized H–C–Cl angle θ varies from a value of 109.0° at $\mathcal{R}$ to a value of 90.0° at ‡. However, Chandrasekhar et al.[6] have optimized the geometries of nine distinct points, for fixed r_c, at the HF/6-31G* level. At this level θ varies from 108.5° at $\mathcal{R}$ to 90.0° at ‡. We chose to fit to these HF/6-31G* values, since they are quite similar to the MP2/6-31G** values, and, since they are available at more geometries, they give more information about the rate of change of θ with respect to r_c in the region near ‡. We used the form

$$\theta^0 = -\gamma_\theta \tanh (a_\theta r_c) + 90° \tag{22}$$

where $\gamma_\theta = 18.5°$ so that $\theta^0(r_c = -\infty) = 108.5°$ and $\theta^0(r_c = +\infty) = 71.5°$, while a_θ was found by a least-squares fit. A value of $a_\theta = 1.36$ Å^{-1} yields a fit to θ^0 which differs from the HF/6-31G* values by less than one-half of a degree at all available points.

For the equilibrium carbon–chlorine distances, we write r^0_{23} as a function of r_c and define $r^0_{12} = r^0_{23}(-r_c)$, to enforce symmetry. This prescription leaves the additional constraint

$$r_c = r^0_{23}(r_c) - r^0_{23}(-r_c) \tag{23}$$

Assuming an exponential form for r^0_{23}—$r^0_{23} = Ae^{\beta r_c} + r^0_{MeCl}$—and applying the constraint eq 23 yields the self-consistent expressions

$$r^0_{23} = A\left\{\frac{r_c}{2A} + \left[\left(\frac{r_c}{2A}\right)^2 + 1\right]^{1/2}\right\} + r^0_{MeCl} \tag{24}$$

$$r^0_{12} = r^0_{23} - r_c = r^0_{23}(-r_c) \tag{25}$$

Equations 24 and 25 require r^0_{23} to have the correct Me–Cl bond length, r^0_{MeCl}, at $r_c = -\infty$ (and r^0_{12} to have this value at $r_c = +\infty$). The parameter A could then be chosen such that $r^0_{12}(0) = r^0_{23}(0)$ has the desired value at ‡. However, this fit does not give the desired carbon–chlorine distances at the complex $\mathcal{C}$. In order to enforce an exact fit to the three-body values of r_{12} and r_{23} at $\mathcal{C}$ (from V^{3B}), we use instead of eq 24 the form

$$r^0_{23} = A\left[\frac{r_c}{2A} + \left(\left(\frac{r_c}{2A}\right)^2 + 1\right)^{1/2}\right] + r^0_{MeCl} + \gamma_r e^{-\beta_r r_c^2} \tag{26}$$

for which both eqs 23 and 25 still hold. Equations 25 and 26 were solved analytically for A, γ_r, and β_r in order that, at $\mathcal{R}$, $\mathcal{C}$, and ‡, r^0_{12} and r^0_{23} equaled, to numerical accuracy, the corresponding r_{12} and r_{23} values at the stationary points of the three-body potential, V^{3B}. The resultant fit, which has the values given in Table VIII, yields r^0_{23} values which differ from the corresponding values on the MEP of V^{3B} by less than 0.03 Å at 26 points considered for 11.224 Å $\geq r_c \geq$ −11.224 Å.

With fits to r^0_H, r^0_{12}, r^0_{23}, and θ^0, we have sufficient information, using symmetry, to evaluate all 18 x_i^0 functions at each value of r_c. In order to evaluate eq 21, we also need fits to the set of Cartesian force constants as a function of r_c. Since the force constant matrix is symmetric, we need only the lower half of the 18 × 18 matrix. To create the functions $\{k_{ij}(r_c)\}$, we begin with the ab initio MP2/6-31G** Cartesian force constant matrices at the three distinct stationary points. However, for reasons discussed previously,[18] we do not attempt to reproduce the ab initio frequencies but rather the ab initio frequencies scaled by a constant value of 0.94, which is an empirical correction factor. Because harmonic force constants are related to the squares of their corresponding frequencies, the force constants must be scaled by a factor of $(0.94)^2 = 0.8836$ in order to reproduce the scaled frequency spectrum.

Because we add V^{vib} to V^{3B}, it needs in principle to account only for interactions involving at least one hydrogen. However, V^{3B} is deficient in some aspects—for example, the bending frequencies are very low, and so we use V^{vib} to correct these deficiencies as well as to introduce the hydrogen interactions. To do this, we rely on the additivity property

$$k^A_{ij} = k^{3B}_{ij} + k^{vib}_{ij} \tag{27}$$

where k^A_{ij}, k^{3B}_{ij}, and k^{vib}_{ij} are the force constants for V_A, for V^{3B}, and for V^{vib}, respectively. Since we desire that k^A_{ij} equal the scaled ab initio force constants, we find the desired force constants for the vibrational potential, $\{k^{vib,d}_{ij}\}$, by replacing k^A_{ij} by scaled MP2/6-31G** force constants in eq 27 and rearranging to give

$$k^{vib,d}_{ij} = 0.8836k^{MP2}_{ij} - k^{3B}_{ij} \tag{28}$$

Notice that in eq 28 k^{3B}_{ij} is zero whenever i or j refers to the coordinate of a hydrogen. We evaluate $\{k^{vib,d}_{ij}\}$ at the three stationary points, ‡, $\mathcal{C}$, and $\mathcal{R}$, which have r_c values defined by the MEP of V^{3B} (which are also consistent with the set $\{x_i^0\}$ and agree with the ab initio values to at least 0.01 Å) and at one intermediate geometry, denoted $\mathcal{I}$, between ‡ and $\mathcal{C}$. The geometry for the point $\mathcal{I}$, taken from the MEP of Chandrasekhar et al., was $r_{12} = 1.906$ Å, $r_{23} = 2.678$ Å, θ (H–C–Cl) = 104.6°, and $r_{CH} = 1.067$ Å. We evaluated the energy and frequencies at this point at the MP2/6-31G** level, which yields an energy of −6.5 kcal/mol relative to $\mathcal{R}$. Because this geometry is not a stationary point, it cannot be unambiguously associated with a point on the MEP of the V^{3B} function. Thus, although $\{k^{vib,d}_{ij}\}$ at this point is associated with a specific value of r_c, in particular $r_c = 0.772$ Å, we do not weight it as heavily when fitting k_{ij} as we weight the three stationary points.

In order to fit all 171 functions, $\{k_{ij}\}$, we split the k_{ij} into groups based on their asymptotic behavior, as illustrated in Figure 7. Due to the symmetric nature of the reaction, force constants which do not involve any chlorine coordinates will be either symmetric, i.e., $k^{vib,d}_{ij}(\mathcal{R}) = k^{vib,d}_{ij}(\mathcal{P})$, or asymmetric, i.e., $k^{vib,d}_{ij}(\mathcal{R}) = -k^{vib,d}_{ij}(\mathcal{P})$ with $k^{vib,d}_{ij}(‡) = 0$, where (‡) refers to $r_c = 0$, the value of r_c at the saddle point. For the symmetric force constants we use the form

$$k_{ij} = k^{vib,d}_{ij}(‡) + [k^{vib,d}_{ij}(\mathcal{P}) - k^{vib,d}_{ij}(‡)]g_{ij}(r_c) \tag{29}$$

where $g_{ij}(‡) = 0$ and $g_{ij}(\mathcal{R}) = g_{ij}(\mathcal{P}) = 1$. This form ensures that the symmetric k_{ij} will exactly equal $k^{vib,d}_{ij}$ at $\mathcal{R}$, $\mathcal{P}$, and ‡. For the asymmetric force constants, we also use eq 29 but with different limits on g_{ij}. In this case $g_{ij}(‡) = 0$ and $g_{ij}(\mathcal{P}) = 1$, but $g_{ij}(\mathcal{R}) = -1$. This again ensures that $k_{ij} = k^{vib,d}_{ij}$ at $\mathcal{R}$, $\mathcal{P}$, and ‡.

The force constants which involve one or the other chlorine atom are not required to exhibit any symmetry as a function of r_c (the three nonzero force constants which involve *both* chlorines do exhibit symmetry and can be fit with eq 29). Instead of eq 29 we use the form

$$k_{ij} = k^{vib,d}_{ij}(\mathcal{R}) + [k^{vib,d}_{ij}(\mathcal{P}) - k^{vib,d}_{ij}(\mathcal{R})]g_{ij}(r_c) \tag{30}$$

where g_{ij} has the limits $g_{ij}(\mathcal{R}) = 0$ and $g_{ij}(\mathcal{P}) = 1$, to fit the nonsymmetric force constants. This form ensures that $k_{ij} = k^{vib,d}_{ij}$ at $\mathcal{R}$ and $\mathcal{P}$.

For all three types of force constants (symmetric, asymmetric, and nonsymmetric) we use the same functional form for g_{ij} but vary the coefficients such that the limits of each g_{ij} are correct for its symmetry type. The form used for g_{ij} is

$$g_{ij} = a_{1,ij} + f_1(r_c;ij) + f_2(r_c;ij) + f_3(r_c;ij) \tag{31}$$

where $a_{1,ij}$ is a constant

$$f_1 = e^{-\beta_{1,ij}(r_c - x_{1,ij})^2}[a_{2,ij} + a_{3,ij}r_c + a_{4,ij}r_c^2] \tag{32}$$

$$f_2 = a_{5,ij} \tanh [\beta_{2,ij}(r_c - x_{2,ij})] \tag{33}$$

and

$$f_3 = r_c\left[a_{6,ij}e^{-(r_c - x_{3,ij})^2} + a_{7,ij}e^{-(r_c + x_{3,ij})^2}\right] \tag{34}$$

The various coefficients were chosen such that g_{ij} has the appropriate limits and $k_{ij} = k^{vib,d}_{ij}$ at $\mathcal{R}$, $\mathcal{C}$, ‡, $\mathcal{C}'$, and $\mathcal{P}$. Any remaining coefficients were fit by a least-squares method to give a reasonable estimate of $k^{vib,d}_{ij}$ at the additional point $\mathcal{I}$. Details

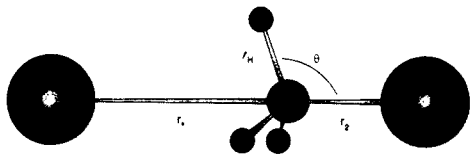

Figure 6. A schematic diagram of the complex $\mathcal{C}$, showing the definitions of the internal coordinates which are used to define the set $\{x_i^0\}$.

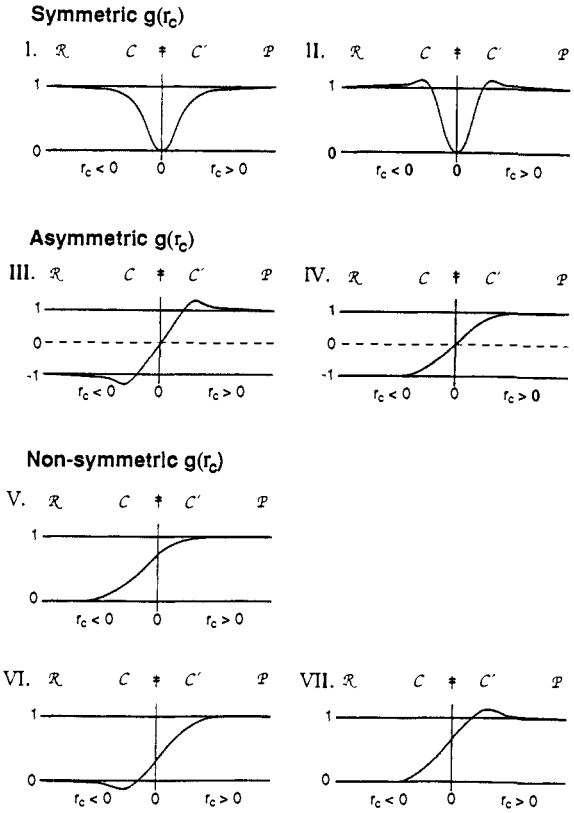

Figure 7. The general shape of g_{ij} for the various types of functions used to fit k_{ij}.

of the fits are given in the Supplementary Material, which also includes a listing of the set of desired force constants, $\{k_{ij}^{\text{vib,d}}\}$.

3. Features and Predictions of Surface A

The full multidimensional surface V_A, which is given by eq 1, correctly shows the three distinct stationary points, $\mathcal{R}$, $\mathcal{C}$, and ‡. The energies and carbon–chloride distances at these points are unchanged from the corresponding values in V^{3B}, Table V. The stationary points exhibit the correct symmetry—C_{3v} at $\mathcal{R}$ and $\mathcal{C}$ and D_{3h} symmetry at ‡. Thus the geometry at each point is defined by the carbon–chlorine distances (given in Table V), the carbon–hydrogen distance r_H, and the angle θ (defined in Figure 6). At all three stationary points, $r_H = 1.07$ Å. The angle θ is 90° at ‡, 107.6° at $\mathcal{C}$, and 108.5° at $\mathcal{R}$ compared with HF/6-31G* values[6] of 90° at ‡, 108.0° at $\mathcal{C}$, and 108.5° at $\mathcal{R}$ and MP2/6-31G** values[18] of 90° at ‡, 109.1° at $\mathcal{C}$, and 109.0° at $\mathcal{R}$. This is illustrated by a plot, Figure 8, of contours vs θ and r_c. In addition, we evaluate the energy of potential V_A at the geometries listed in Table VII, in order to ascertain whether we have altered the shape of the potential in the vicinity of the reaction path from that of V^{3B} (in the relevant dimensions). For each collinear geometry in Table VII, given by r_{12} and r_{23}, which define r_c, we place the hydrogen atoms at their equilibrium positions, as defined by $\{x_i^0\}$. From the results in Table VII, it is clear that the qualitative shape of surface A is very similar to that of V^{3B} in this region. Quantitatively, we see that at all points potential V_A yields somewhat more accurate energies, as compared to the ab initio results, than does V^{3B}.

In Table IX we list the frequencies of potential V_A at the three stationary points. For comparison, we have also listed the scaled

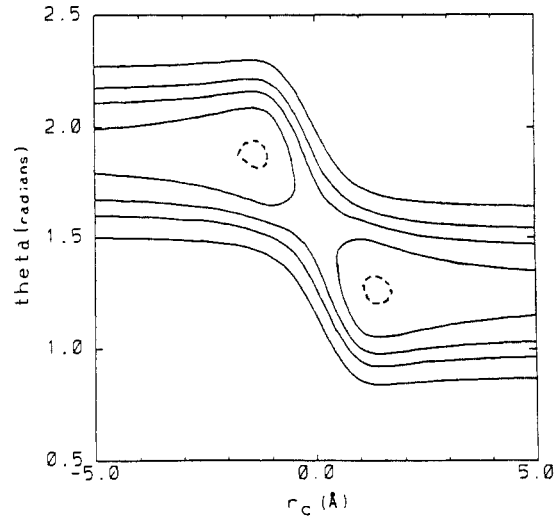

Figure 8. A contour plot for potential function V_A in the variables of θ (defined in Figure 6) and r_c, with all other coordinates in their equilibrium positions. Energy contours are at −10, 0, 10, 20, and 40 kcal/mol.

Table IX. Frequencies (in cm^{-1}) from Surface A, from Scaled ab Initio Calculations (ref 18), and from Experiment (ref 30)

	A	scaled MP2/6-31G**	expt
		$\mathcal{R}$	
a_1	741	741	732
e	1017	1017	1017
a_1	1377	1377	1355
e	1453	1453	1452
a_1	2981	2981	2937
e	3092	3092	3039
		$\mathcal{C}$	
e	68	68	
a_1	113	107	
a_1	702	653	
e	971	971	
a_1	1307	1312	
e	1429	1429	
a_1	3034	3032	
e	3154	3155	
		‡	
a_2''	496i	485i	
e'	206	206	
a_1'	220	220	
e''	947	947	
a_2''	1021	1021	
e'	1381	1381	
a'	3106	3106	
e'	3309	3309	

MP2/6-31G** ab initio frequencies for each stationary point.[18] At $\mathcal{R}$, we also include recent experimental values.[30] The frequencies of potential V_A are quite good. For the reactants, all of the frequencies of our fit agree with the scaled ab initio values to within 1 cm^{-1}. These frequencies agree with the experimental values to 2% or better. At the complex, all but two of the frequencies of the fit agree with the scaled ab initio values to better than 1%. The very low frequency a_1 asymmetric stretch is 6% higher than the scaled ab initio value of 107 cm^{-1}, and the a_1 frequency that will become the a_1' symmetric stretch frequency at ‡ is 7% higher than the scaled ab initio value of 653 cm^{-1}. At ‡, all bound frequencies agree with the scaled ab initio values to within 1 cm^{-1}, and the imaginary frequency is just 2% high.

The scaled value, 485i cm^{-1}, of the imaginary frequency at the saddle point is very similar to the value of 460i cm^{-1} for this imaginary frequency on the model potential energy surface of ref 8.

Table X gives generalized transition-state theory rate constants for this potential energy function at four successively refined levels of approximation:[39-44] conventional transition-state theory (TST),

Table X. Calculated Rate Constants in cm^3 $molecule^{-1}$ s^{-1}

surface	T (K)	conventional TST	CVT	CVT/MEPSAG	CVT/SCSAG
A	250	4.2 (−16)	4.1 (−16)	6.3 (−16)	8.2 (−16)
	300	2.1 (−15)	2.1 (−15)	2.8 (−15)	3.3 (−15)
	500	7.6 (−14)	7.3 (−14)	8.1 (−14)	8.6 (−14)
	1000	2.0 (−12)	2.0 (−12)	2.0 (−12)	2.0 (−12)
S	250	7.5 (−15)	7.3 (−15)	1.1 (−14)	1.4 (−14)
	300	2.4 (−14)	2.3 (−14)	3.0 (−14)	3.5 (−14)
	500	3.2 (−13)	3.1 (−13)	3.4 (−13)	3.6 (−13)
	1000	4.2 (−12)	4.0 (−12)	4.1 (−12)	4.2 (−12)

canonical variational TST (CVT), CVT combined with a semiclassical adiabatic ground-state (SAG) transmission coefficient based on tunneling along the minimum energy path (MEPSAG), and CVT combined with the small-curvature semiclassical adiabatic ground-state (SCSAG) transmission coefficient. The SCSAG tunneling calculation differs from the MEPSAG one in that it allows corner cutting[45,46] during tunneling.

We find that variational effects are negligible, as a consequence of the fact that the vibrational frequencies change only slowly along the reaction path in the vicinity of the saddle point. Thus, the CVT rate constant is virtually the same as the conventional TST rate constant at all temperatures in Table X. Perhaps surprisingly, the SCSAG transmission coefficient increases the rate by a factor of 2 at 250 K, i.e., the tunneling contribution is approximately equal to the overbarrier one. The increase due to tunneling as evaluated by the less accurate MEPSAG method at 250 K is only 54%, indicating that corner cutting of the tunneling path is important in this multidimensional reaction. It is interesting to note that if we calculate reaction rates on the three-body potential, V^{3B}, where the hydrogens are not treated explicitly and their motion cannot couple to the reaction coordinate motion, the MEPSAG and the SCSAG tunneling corrections yield increases of 33% and 40%, respectively, which are both of similar magnitude to the MEPSAG correction for the multidimensional potential function V_A. Thus, we see that corner cutting of the tunneling path is of much greater importance when the hydrogen motions are included explicitly. The effects of the tunneling corrections follow the same trends at 300 K, but they are smaller in magnitude. For example, for multidimensional potential function V_A, the MEPSAG corrections increases the rate by 33%, while the SCSAG correction increases the rate by 57%. At 500 K these quantum corrections are only 11% and 18%, respectively. We note that significant tunneling of heavy groups has been observed recently in other theoretical calculations of organic reactions.[47-51] It would be interesting to determine to what extent this tunneling can be associated with methyl hydrogens and/or with heavy group motions, but we have not done so.

Table XI. Frequencies for Potential Function V_S

	R		
a_1	741	e	1453
e	1017	a_1	2981
a_1	1377	e	3092
	C		
e	68	a_1	1305
a_1	113	e	1429
a_1	698	a_1	3035
e	970	e	3155
	‡		
a_2''	469i	a_2''	1021
e'	206	e'	1381
a_1'	220	a_1'	3106
e''	947	e'	3309

Table XII. Rate Constants and Activation Energies Calculated by the CVT/SCSAG Method for Potential Function V_S

T (K)	k (cm^3 $molecule^{-1}$ s^{-1})	E_a (kcal/mol)	T (K)	k (cm^3 $molecule^{-1}$ s^{-1})	E_a (kcal/mol)
200	4.1 (−15)	2.2	450	2.3 (−13)	3.8
250	1.4 (−14)	2.6	500	3.6 (−13)	4.1
300	3.5 (−14)	3.0	600	7.3 (−13)	4.5
350	7.5 (−14)	3.3	800	2.0 (−12)	5.3
400	1.4 (−13)	3.6	1000	4.2 (−12)	6.0

The Arrhenius energy of activation, E_a, calculated from the CVT/SCSAG rate constants by

$$E_a = RT^2\, d(\ln k)/dT \tag{35}$$

is a function of temperature. It was evaluated by numerical differentiation of rate constants calculated at closely spaced pairs of temperatures. It equals 4.0 kcal/mol at 250 K and 7.5 kcal/mol at 1000 K.

Our best estimate of the rate at 300 K for this potential gives 3.3×10^{-15} cm^3 $molecule^{-1}$ s^{-1}, and the experimental value[21] is 11 times larger, 3.5×10^{-14} cm^3 $molecule^{-1}$ s^{-1}. We believe that this discrepancy results because the MP2/6-31G** barrier height is somewhat high. In the following section, we discuss a semiempirical correction to the surface V_A which brings the CVT/SCSAG rate constant up to the experimental result at 300 K.

4. A Semiempirical Surface

Because we believe that the MP2/6-31G** barrier, $\Delta E^* = 4.5$ kcal/mol, is too high,[18] we create a semiempirical surface, V_S, in which the barrier is adjusted such that it yields a CVT/SCSAG rate constant at 300 K which is in agreement with the experimental result.

The semiempirical surface is related to the ab initio surface V_A by the relation eq 2, where V_δ is a function only of r_c. It is given by

$$V_\delta = \Delta E_b e^{-\beta r_c^2} \tag{36}$$

where ΔE_b is the change in the barrier height required for V_S to yield the experimental rate constant at 300 K. This form was chosen because it enables us to vary the barrier height without affecting the properties of the complex or the reactants to any large degree. Since our goal is to make the minimum changes necessary to correct the error in the predicted rate constants, assuming both the correctness of the experiment and the validity of our generalized transition-state theory calculations, and since

(36) Miller, T. M.; Bederson, B. In *Advances in Atomic and Molecular Physics*; Bates, D. R., Bederson, B., Eds.; Academic Press: New York, 1977; Vol. XIII, p 49.
(37) McEachran, R. P.; Stauffer, A. D.; Greita, S. *J. Phys. B* **1979**, *12*, 3119.
(38) Hirschfelder, J. O.; Curtiss, C. F.; Bird, R. B. *Molecular Theory of Gases and Liquids*; John Wiley & Sons: New York, 1954; p 950.
(39) Garrett, B. C.; Truhlar, D. G.; Grev, R. S.; Magnuson, A. W. *J. Phys. Chem.* **1980**, *84*, 1730; **1983**, *87*, 4554E.
(40) Skodje, R. T.; Truhlar, D. G.; Garrett, B. C. *J. Phys. Chem.* **1981**, *85*, 3019.
(41) Truhlar, D. G.; Isaacson, A. D.; Skodje, R. T.; Garrett, B. C. *J. Phys. Chem.* **1982**, *86*, 2252; **1983**, *87*, 4554E.
(42) Truhlar, D. G.; Isaacson, A. D.; Garrett, B. C. In *The Theory of Chemical Reaction Dynamics*; Baer, M., Ed.; CRC Press: Boca Raton, FL, 1985; p 65.
(43) Isaacson, A. D.; Sund, M. T.; Rai, S. N.; Truhlar, D. G. *J. Chem. Phys.* **1985**, *82*, 1338.
(44) Tucker, S. C.; Truhlar, D. G. In *New Theoretical Concepts for Understanding Organic Reactions*; Bertrán, J., Csizmadia, I. G., Eds.; Kluwer: Dordrecht, 1989; p 291.
(45) Marcus, R. A. *J. Chem. Phys.* **1966**, *45*, 4493; **1969**, *49*, 2617.
(46) Skodje, R. T.; Truhlar, D. G.; Garrett, B. C. *J. Chem. Phys.* **1982**, *77*, 5955.
(47) Dewar, M. J. S.; Merz, K. M., Jr.; Stewart, J. J. P. *J. Am. Chem. Soc.* **1984**, *106*, 4040.
(48) Huang, M.-J.; Wolfsberg, M. *J. Am. Chem. Soc.* **1984**, *106*, 4039.
(49) Carpenter, B. K. *J. Am. Chem. Soc.* **1983**, *105*, 1700.
(50) Saunders, M.; Johnson, C. S. *J. Am. Chem. Soc.* **1987**, *109*, 4401.
(51) Sponsler, M. B.; Jain, R.; Coms, F. D.; Dougherty, D. A. *J. Am. Chem. Soc.* **1989**, *11*, 2240.

Table XIII. Rate Constants and Activation Energies for the Reaction of Cl^- with CD_3Cl Calculated by the CVT/SCSAG Method for Potential Function V_S

T (K)	k (cm^3 molecule^{-1} s^{-1})	E_a (kcal/mol)	T (K)	k (cm^3 molecule^{-1} s^{-1})	E_a (kcal/mol)
200	4.3 (−15)	2.2	450	2.4 (−13)	3.8
250	1.4 (−14)	2.6	500	3.8 (−13)	4.1
300	3.7 (−14)	3.0	600	7.7 (−13)	4.5
350	7.8 (−14)	3.3	800	2.1 (−12)	5.3
400	1.4 (−13)	3.6	1000	4.4 (−12)	6.0

the calculated complexation energy agrees with experiment to within experimental error (see section 2.1), we localize the change in the vicinity of the saddle point. Thus we fit the width parameter β_δ to make the gaussian V_δ as broad (and hence smooth) as possible, without allowing the geometry of the complex to be altered (to 0.01 Å). This ensures that the rate of decay of the long-range forces between $\mathcal{C}$ and $\mathcal{R}$ will not be noticeably affected by the modification V_δ. We found that these criteria were met by $\beta_\delta = 2.0$ Å^{-2}. With this width parameter, a barrier change of $\Delta E_b = -1.43$ kcal/mol, leading to a barrier for surface V_S of $\Delta E^\ddagger = 3.10$ kcal/mol, yields a CVT/SCSAG rate constant at 300 K of 3.5×10^{-14} cm^3 $molecule^{-1}$ s^{-1}, in agreement with the experimental[21] result.

In Table X, we present the conventional, CVT, CVT/MEPSAG, and CVT/SCSAG rate constants for potential function V_S at four temperatures. The trends are the same as for potential function V_A. The frequencies for V_S at $\mathcal{R}$, $\mathcal{C}$, and ‡ are given in Table XI. As desired, there is no difference between the frequencies for V_S and V_A (Table IX) at $\mathcal{R}$. At $\mathcal{C}$ only one frequency differs by more than 2 cm^{-1} from the corresponding frequencies of V_A, and this by less than 1%. At ‡, only the imaginary frequency differs by more than 1 cm^{-1} from the corresponding frequency of V_A. The imaginary frequency is 469i cm^{-1}, which is 5% lower than the imaginary frequency of V_A. This change is consistent with the lower barrier of V_S since a lower barrier will not be as steep and hence will have a smaller negative force constant.

Having semiempirically adjusted the barrier height we are now in a position to more realistically estimate the phenomenological energy of activation, also called the Arrhenius activation energy, as defined by eq 35. The rate constants and activation energies are tabulated in Table XII. The activation energy is predicted to increase by a factor of 2.7 over the temperature range studied. It will be interesting to see how well these predictions agree with experiment when the rate constant for R1 is measured as a function of temperature.

Another quantity predicted by these calculations, but which also has not been measured yet, is the kinetic isotope effect for perdeuteration, i.e., the ratio of the reaction rate for CD_3Cl to that for CH_3Cl. We give the CVT/SCSAG rate constants and activation energies for the reaction of Cl^- with CD_3Cl in Table XIII. We predict a kinetic isotope effect of 1.04 at 300 K from calculations with three different methods, conventional TST, CVT, and CVT/SCSAG. Since these three results are so similar, variational transition-state effects and tunneling do not contribute appreciably to the kinetic isotope effect. To understand the effect, the ratio of partition functions in the generalized transition-state theory rate constant expression is written as a product of a vibrational ratio, a rotational ratio, and a translational ratio. The vibrational ratio (the generalized transition-state vibrational partition function divided by the reactant vibrational partition function) for the reaction of CD_3Cl is 32% greater than the corresponding ratio for the reaction of CH_3Cl, yielding a multiplicative contribution to the kinetic isotope effect of 1.32. The vibrational contribution is largely cancelled by the rotational contribution to the kinetic isotope effect of 0.82; the net contribution of the product of these factors is 1.08. The remaining contribution, from the ratios of translational partition functions, although near unity at 0.97, further cancels part of the large vibrational contribution, to yield the final calculated kinetic isotope effect of 1.04. We note that if we perform the calculation by using *classical* vibrational partition functions, the vibrational contribution to the kinetic isotope effect is 1.27, slightly smaller than with quantum partition functions, and it is completely cancelled by the rotational and translational contributions, causing the classical kinetic isotope ratio to be 1.00. The kinetic isotope effect evaluated with the semiclassical CVT/SCSAG method varies from 1.07 at 200 K down to 1.04 at 300 K, back up to 1.05 at 600 K, and finally down to 1.03 at 1500 K; i.e., we predict a small kinetic isotope effect which is generally decreasing as a function of temperature. Again the comparison to future experiments will be very interesting. (Although the kinetic isotope effect has not been measured in the gas phase, our value is remarkably, perhaps fortuitously, close to the value of 1.03 obtained[4] by Marcus theory from data on kinetics in solution.)

5. Conclusion

In this work we have presented two multidimensional potential energy functions for the gas-phase chloride exchange reaction, $Cl^- + CH_3Cl \rightarrow ClCH_3 + Cl^-$, in which all six atoms are treated explicitly. One function is fit entirely to ab initio energies, geometries, and frequencies at the reactants, charge–dipole complex, transition state, and additional geometries in the repulsive region and near the reaction path. The second surface is similar to the first, but it contains a semiempirical correction to the barrier region such that the generalized transition-state theory rate constant at 300 K, as calculated by the CVT/SCSAG semiclassical variational transition-state theory method, agrees with the experimental value.

For both surfaces the frequencies orthogonal to the minimum energy path vary smoothly from the reactants to the precursor ion–dipole complex to the transition state to the successor ion–dipole complex to the products, and all of the bound frequencies at the stationary points agree with the scaled ab initio values to 1% or better, except for two low-energy frequencies at the ion–dipole complex which differ from the scaled ab initio values by 6% and 7%, respectively. For the first potential function the frequency of the unbound mode at the saddle point differs from the scaled ab initio value by only 2%.

An important aspect of both of these functions is that, because the vibrational interactions were fit in Cartesian rather than internal coordinates, and we fit directly to the full Cartesian second derivative matrix from scaled ab initio calculations, no assumptions were made, either implicitly through a choice of interaction terms in internal coordinates or explicitly to simplify functional forms, about which, if any, mode coupling terms could be neglected—they are all included.

The rate constants for these potential functions, calculated by variational transition-state theory with semiclassical tunneling contributions, indicate that variational effects (i.e., effects due to deviations of variational transition states from a saddle point) are negligible for this reaction at room temperature. Tunneling effects, however, were larger than expected, causing nearly a 60% increase in the rate at 300 K when evaluated by the small-curvature semiclassical adiabatic ground-state (SCSAG) method with the semiempirical potential function. A comparison of the tunneling correction evaluated assuming zero curvature of the reaction path to that evaluated by the SCSAG method indicates that slightly under half of this tunneling correction is due to curvature coupling between the reaction coordinate and the generalized normal modes orthogonal to the reaction path. We also predicted the temperature dependence of the Arrhenius activation energy, which we find to increase from 2.2 kcal/mol at 200 K to 6.0 kcal/mol at 1000 K, indicating a very curved Arrhenius plot.

We hope that the existence of a full 18-dimensional potential energy surface for this six-body reaction will enable more realistic dynamical simulations of solvation and microsolvation effects, and we report the first such usage of the new energy surface in the following paper,[17] where we study the effect of microsolvation on this reaction. Another interesting application would be to test

the sensitivity of recent conclusions[16] about mode selectivity in S_N2 reactions to variations in the potential energy function.

Acknowledgment. We are grateful to Maurice Kreevoy for helpful discussions. This work was supported in part by the U.S. Department of Energy, Office of Basic Energy Sciences and the Minnesota Supercomputer Institute.

Registry No. Cl, 16887-00-6; CH_3Cl, 74-87-3; D, 7782-39-0; Cl_2, 7782-50-5.

Supplementary Material Available: A description of the method used to determine the coefficients for g_{ij}, eq 31, and a listing of the force constant matrix (16 pages). Ordering information is given on any current masthead page.

Effect of Nonequilibrium Solvation on Chemical Reaction Rates. Variational Transition-State-Theory Studies of the Microsolvated Reaction $Cl^-(H_2O)_n + CH_3Cl$

Susan C. Tucker and Donald G. Truhlar*

Contribution from the Department of Chemistry and Supercomputer Institute, University of Minnesota, Minneapolis, Minnesota 55455-0431. *Received July 24, 1989*

Abstract: We present a potential energy surface for the microhydrated S_N2 reaction of a chloride ion with methyl chloride in the presence of one or two water molecules. All degrees of freedom are included. We analyze the stationary points corresponding to reactant, ion–dipole complex, and transition state for the monohydrated and the dihydrated reactions, and we use generalized transition-state theory to evaluate the rate constants for these reactions. A noteworthy feature of the dynamics calculations is that vibrational zero point effects are included, as are effects of quantization on vibrational heat capacities and entropies, and water molecules are treated as nonrigid. We find that the rate constant at 300 K decreases from the gas-phase value of 3.5×10^{-14} cm^3 molecule^{-1} s^{-1} to a value of 1.1×10^{-17} cm^3 molecule^{-1} s^{-1} for the monohydrated reaction and to a value of 3.7×10^{-20} cm^3 molecule^{-1} s^{-1} for the dihydrated reaction. We have also evaluated the rate constant for the monohydrated reaction under the equilibrium solvation approximation. The extent of nonequilibrium solvation is tested by comparing calculations in which the water molecule degrees of freedom participate in the reaction coordinate to those in which they do not. Two different methods for defining the generalized transition-state theory dividing surface under the equilibrium solvation approximation lead to quite different values for the equilibrium solvation rate constant, and we determine which equilibrium solvation approximation is more appropriate by using variational transition-state theory.

1. Introduction

The study of solvent effects on chemical reaction rates has a long history, and it has played a central role in recent work examining the applicability of transition-state theory to reactions in solution, as discussed in recent reviews.[1-3] Theoretical interpretation of bimolecular nucleophilic substitution (S_N2) reactions also has a long history,[4,5] and these reactions have become the prototype for recent work on solvent effects. In particular, the reaction of chloride with methyl chloride has received considerable recent attention.[6-22] Two strong themes distinguishing the modern work from the classical studies[23] are (i) the comparison of ionic reaction kinetics in solution to data on the same reactions as they occur with uncomplexed reagents in the gas phase[8-15,21,22] and (ii) quantitative studies of microsolvated species, i.e., clusters, as a bridge between the gas phase and solution.[6,11,24-29] This paper is a detailed study of the effect of microsolvation, in particular microhydration, on the prototype S_N2 reaction of chloride and methyl chloride, using variational transition-state theory (VTST)[1,3,13,16,17,30-35] and a potential energy surface in which all

(1) Truhlar, D. G.; Hase, W. L.; Hynes, J. T. *J. Phys. Chem.* **1983**, *87*, 2664, 5523(E).
(2) Hynes, J. T. In *Theory of Chemical Reaction Dynamics*; Baer, M., Ed.; CRC Press: Boca Raton, FL, 1985; Vol. 4, p 171.
(3) Kreevoy, M. M.; Truhlar, D. G. In *Investigation of Rates and Mechanisms of Reactions* (*Techniques of Chemistry*, 4th ed.; Weissberger, A., Ed.; Vol. 6) Bernasconi, C. F., Ed.; John Wiley & Sons: New York, 1986; Part I, p 13.
(4) Dostrovsky, I.; Hughes, E. D.; Ingold, C. K. *J. Chem. Soc.* **1946**, 173.
(5) de la Mare, P. B. D.; Fowden, L.; Hughes, E. D.; Ingold, C. K., Mackie, J. D. H. *J. Chem. Soc.* **1955**, 3200.
(6) Morokuma, K. *J. Am. Chem. Soc.* **1982**, *104*, 3732.
(7) Bazilevskii, M. V.; Koldobskii, S. G. *Zh. Org. Khim.* **1984**, *20*, 908.
(8) Chandrasekhar, J.; Smith, S. F.; Jorgensen, W. L. *J. Am. Chem. Soc.* **1985**, *107*, 154.
(9) Shaik, S. S. *Prog. Phys. Org. Chem.* **1985**, *15*, 197.
(10) German, E. D.; Kuznetsov, A. M. *Faraday Trans. II* **1986**, *82*, 1885.
(11) Kong, Y. S.; Jhon, M. S. *Theor. Chim. Acta* **1986**, *70*, 123.
(12) Bergsma, J. P.; Gertner, B. J.; Wilson, K. R.; Hynes, J. T. *J. Chem. Phys.* **1987**, *86*, 1356.
(13) Gertner, B. J.; Bergsma, J. P.; Wilson, K. R.; Lee, S.; Hynes, J. T. *J. Chem. Phys.* **1987**, *86*, 1377.
(14) Bash, P. A.; Field, M. J.; Karplus, M. *J. Am. Chem. Soc.* **1987**, *109*, 8092.
(15) Burshtein, K. Y. *J. Mol. Struct.* **1987**, *153*, 209.
(16) Lee, S.; Hynes, J. T. *J. Chem. Phys.* **1983**, *88*, 6863.
(17) Hwang, J.-K.; King, G.; Creighton, S.; Warshel, A. *J. Am. Chem. Soc.* **1988**, *110*, 5297.
(18) Hwang, J.-K.; Creighton, S.; King, G.; Whitney, D.; Warshel, A. *J. Chem. Phys.* **1988**, *89*, 859.
(19) Gertner, B. J.; Wilson, K. R.; Hynes, J. T. *J. Chem. Phys.* **1989**, *90*, 3537.
(20) Kozaki, T.; Morishashi, K.; Kikuchi, O. *J. Am. Chem. Soc.* **1989**, *111*, 1547.
(21) Chiles, R. A.; Rossky, P. J. *J. Am. Chem. Soc.* **1984**, *106*, 6867. Huston, S. E.; Rossky, P. J.; Zichi, D. A. *J. Am. Chem. Soc.* In press.
(22) Tucker, S. C.; Truhlar, D. G. *Chem. Phys. Lett.* **1989**, *157*, 164.
(23) Hine, J. *Physical Organic Chemistry*; McGraw-Hill: New York, 1962.
(24) Bertrán, J. In *New Theoretical Concepts for Understanding Organic Reactions*, *NATO ASI Ser. C*; Bertrán, J., Csizmadia, I. G., Eds.; Kluwer Academic Publishers: Dordrecht, 1989, Vol. 267, p 231.
(25) Bohme, D. K.; Raskit, A. B. *J. Am. Chem. Soc.* **1984**, *106*, 3447.
(26) Bohme, D. K.; Raskit, A. B. *Can. J. Chem.* **1985**, *63*, 3007.
(27) Henchman, M.; Paulson, J. F.; Hierl, P. M. *J. Am. Chem. Soc.* **1983**, *105*, 5509.
(28) Henchman, M.; Hierl, P. M.; Paulson, J. F. *J. Am. Chem. Soc.* **1985**, *107*, 2812.
(29) Henchman, M.; Hierl, P. M.; Paulson, J. F. *ACS Adv. Chem. Ser.* **1987**, *215*, 83.

0002-7863/90/1512-3347$02.50/0